Author Manuscript

Author Manuscript

Author Manuscript

Author Manuscript

HHS Public Access

Author manuscript

Cancer Res. Author manuscript; available in PMC 2018 November 01.

Published in final edited form as:

Cancer Res. 2017 November 01; 77(21): 5795–5807. doi:10.1158/0008-5472.CAN-17-1325.

Genetic dissociation of glycolysis and the TCA cycle affects neither normal nor neoplastic proliferation

Laura E. Jackson[a], **Sucheta Kulkarni**[b], **Huabo Wang**[b], **Jie Lu**[b], **James M. Dolezal**[b], **Sivakama S. Bharathi**[c], **Sarangarajan Ranganathan**[d], **Mulchand S. Patel**[e], **Rahul Deshpande**[f], **Frances Alencastro**[g], **Stacy G. Wendell**[f], **Eric S. Goetzman**[c], **Andrew W. Duncan**[g], and **Edward V. Prochownik**[b,h,i,1]

[a]Divisions Neonatology, Children's Hospital of Pittsburgh of The University of Pittsburgh Medical Center (UPMC), Pittsburgh, PA 15224

[b]Hematology/Oncology, Children's Hospital of Pittsburgh of The University of Pittsburgh Medical Center (UPMC), Pittsburgh, PA 15224

[c]Medical Genetics, Department of Pediatrics, Children's Hospital of Pittsburgh of The University of Pittsburgh Medical Center (UPMC), Pittsburgh, PA 15224

[d]Department of Pathology, Children's Hospital of Pittsburgh of UPMC, Pittsburgh, PA 15224

[e]Department of Biochemistry, Jacobs School of Medicine and Biomedical Sciences, University at Buffalo, The State University of New York, Buffalo, NY 14228

[f]Department of Pharmacology and Chemical Biology, University of Pittsburgh School of Medicine, Pittsburgh, PA 15213

[g]Department of Pathology, The McGowan Institute for Regenerative Medicine and The Pittsburgh Liver Research Center, UPMC, Pittsburgh, PA 15213

[h]Department of Microbiology and Molecular Genetics, UPMC

[i]The University of Pittsburgh Cancer Institute, Pittsburgh, PA 15232

Abstract

Rapidly proliferating cells increase glycolysis at the expense of oxidative phosphorylation (oxphos) to generate sufficient levels of glycolytic intermediates for use as anabolic substrates. The pyruvate dehydrogenase complex (PDC) is a critical mitochondrial enzyme that catalyzes pyruvate's conversion to acetyl coenzyme A (AcCoA), thereby connecting these two pathways in response to complex energetic, enzymatic and metabolic cues. Here we utilized a mouse model of hepatocyte-specific PDC inactivation to determine the need for this metabolic link during normal hepatocyte regeneration and malignant transformation. In PDC "knockout" (KO) animals, the long-term regenerative potential of hepatocytes was unimpaired, and growth of aggressive experimental hepatoblastomas (HB) was only modestly slowed in the face of 80–90% reductions in AcCoA and significant alterations in the levels of key TCA cycle intermediates and amino acids. Overall, oxphos activity in KO livers and HB was comparable to that of control

[1]Correspondence: Edward V. Prochownik, M.D., Ph.D. Division of Hematology/Oncology, Children's Hospital of Pittsburgh of UPMC, Pittsburgh, PA 15224, Tel: (412) 692-6795, procev@chp.edu.

Author Manuscript Author Manuscript Author Manuscript Author Manuscript

counterparts, with evidence that metabolic substrate abnormalities were compensated for by increased mitochondrial mass. These findings demonstrate that the biochemical link between glycolysis and the TCA cycle can be completely severed without affecting normal or neoplastic proliferation, even under the most demanding circumstances.

Keywords

hepatoblastoma; tumor metabolism; pyruvate dehydrogenase complex

Introduction

Tumors and rapidly dividing normal tissues must confront several metabolic challenges not ordinarily faced by quiescent cells. First, they must synthesize or otherwise provide anabolic precursors to support their growth and proliferation (1,2). Second, they must generate sufficient amounts of ATP to drive the *de novo* synthesis or uptake of these precursors and their subsequent assembly into macromolecules (1,3). Finally, and particularly in the case of tumors, they must often accomplish these tasks within the confines of hypoxic, acidotic and nutrient-deprived environments (4). The point at which these activities and conditions become rate limiting for growth can vary among different tumor types and even within the same tumor over relatively short times and distances (5) thus requiring tumors to accommodate to often conflicting metabolic demands.

One way by which dividing cells can provide biosynthetic precursors is by increasing the uptake and utilization of environmentally-derived glucose for purposes other than energy production. This process, known as the Warburg effect, occurs under aerobic conditions and allows for the synthesis of anabolic precursors from glycolytic intermediates without necessarily compromising ATP supply (1). Several strategies may be adopted to potentiate the Warburg effect, including regulation of the pyruvate dehydrogenase complex (PDC), a large multi-component enzyme complex that irreversibly catalyzes the intra-mitochondrial oxidative decarboxylation of pyruvate to acetyl coenzyme A (AcCoA), CO_2 and NADH. As the link between glycolysis and the TCA cycle, the PDC has been proposed to be a regulator of the Warburg effect and a gatekeeper for energy production in general (6,7). The PDC also generates NADH to drive oxidative phosphorylation (Oxphos) via the electron transport chain (ETC), the primary source of ATP under normoxic conditions. Efficient communication between glycolysis and the TCA cycle, coupled with the ability to rapidly shift between the two processes according to cellular and environmental circumstances, likely contributes to metabolic adaptability and survival of tumors and normal proliferating cells alike.

The PDC is comprised of three components referred to as pyruvate dehydrogenase (E1), dihydrolipoyl acetyltransferase (E2), and dihydrolipoyl dehydrogenase (E3) (7), and is subject to complex regulation that occurs largely through the E1 component, a hetero-tetramer comprised of 2α and 2β subunits encoded by the *PDHA1* gene [hereafter PDHα (or E1α) and PDHβ (or E1β)]. E1 activity is regulated primarily by phosphorylation/dephosphorylation of the PDHα subunit that is mediated by the inhibitory PDH-kinase

Author Manuscript Author Manuscript Author Manuscript Author Manuscript

(PDK1) and the stimulatory PDH-phophatase (PDP2). These activities, in turn, are themselves modulated in opposite ways by the prevailing levels of intra-mitochondrial ATP, AMP and other metabolites such as NADH, AcCoA and PEP (6,7).

In keeping with the presumed centrality of the PDC in metabolism, total body deletion of the *Pdha1* gene in mice is embryonic lethal (8). Naturally occurring *PDHA1* gene mutations in humans are associated with variable levels of residual enzymatic activity, suggesting that complete inactivation is, as in the mouse, incompatible with survival (9). PDH deficiency typically presents with varying degrees of lactic acidosis, the severity of which correlates inversely with residual enzymatic activity (9). In contrast, mice with conditional, liver-specific deletion of the *Pdha1* gene are born at expected Mendelian frequencies, breed normally, and show only modestly increased whole body insulin sensitivity (10). The survival differences between global and tissue-restricted *Pdha1* "knockout" (KO) mice may reflect differential tissue dependencies on PDC enzymatic activity and/or the ability of individuals with residual enzymatic activity in other tissues to metabolize lactate, thereby avoiding the lethal consequences of uncompensated lactic acidosis.

The idea that the PDC plays an important role in tumorigenesis has been suggested by our recent findings that the enzyme's activity is significantly up-regulated in genetically distinct murine models of liver cancer, namely hepatoblastoma (HB) and hepatocellular carcinoma (HCC); this was shown by direct enzymatic assays in addition to western blot analysis illustrating the loss of phosphorylated PDHα, in addition to an increase in the stimulatory phosphatase and a decrease in the inhibitory kinase (11–13). We proposed that up-regulating PDC activity might represent an attempt by these tumors to maximize the mitochondrial delivery and utilization of limited amounts of pyruvate given the intense competition for upstream glycolytic intermediates by anabolic pathways.

In the current work, we have examined how conditional genetic ablation of *Pdha1* affects long-term proliferative potential of normal and neoplastic hepatocytes. In the former case, we utilized a murine model of type I hereditary tyrosinemia in which intra-splenically transplanted donor hepatocytes gradually replace the affected recipient hepatic parenchyma (14,15). This approach affords several advantages over the more conventional partial hepatectomy (PH) model. First, donor hepatocyte proliferation occurs over a 3–5 month period versus 7–10 days in PH. Second, depending on the inoculum size, donor hepatocytes replicate 50–100 fold as they replace the recipient parenchyma, whereas replication following PH involves, on average, fewer than two cell doublings (15,16). Finally, hepatocyte transplants can be performed competitively with mixed donor cell populations, thereby providing an exceedingly sensitive way of documenting small differences in long-term repopulation potential (14), while ensuring that the *in vivo* environments of the donor populations are identical.

In the case of neoplastic proliferation, we utilized two variations of the above-mentioned model of HB (11,12). In the first, hydrodynamic tail vein injection (HDTVI) of "Sleeping Beauty" plasmids encoding mutant forms β-catenin and yes-associated protein (YAP) (11,12) were performed in mice bearing a conditional, pan-hepatocyte knockout (pKO) of the *Pdha1* gene (Fig. 1A). A second model was utilized in parallel in which mice with intact

Author Manuscript Author Manuscript Author Manuscript Author Manuscript

loxP sites flanking the *Pdha1* locus (and hereafter referred to as control mice) were inoculated with the same Sleeping Beauty vectors plus an additional Cre recombinase vector, thus allowing for the targeted deletion of the *Pdha1* locus only in hepatocytes destined to become transformed (Fig. 1B). We refer to tumors arising in this background as "restricted knockout" (rKO).

Using a combination of the above-described approaches, we demonstrate that both normal and neoplastic hepatocyte proliferation remain largely unimpaired by the absence of the PDC. We explore the accompanying biochemical and metabolic adaptations and suggest how they potentially compensate for the loss of this key enzyme. Collectively, our results demonstrate unequivocally that the link between glycolysis and the TCA cycle can be genetically severed with little impact on proliferative potential.

Materials and Methods

Animal studies

All animal work was performed in conformity with the Public Health Service Policy on Humane Care and Use of Laboratory Animal Research (DLAR) Guide for Care and Use of Laboratory Animals. All procedures were reviewed and approved by the Institutional Animal Care and Use Committee (IACUC) at the University of Pittsburgh (protocol #14104886). All mice were housed in a pathogen-free facility and maintained under standard conditions with *ad lib* access to food and water. Homozygous *Pdha1*^{flox8} ("floxed") female mice, which have two loxP sequences flanking exon 8 (8), were bred with male mice containing cre recombinase under the liver-specific albumin promoter (Alb-cre). This procedure yielded mice with a deleted exon 8, which are referred to as KO or "pan KO" (pKO) mice to connote the hepatocyte-wide knockout (14). Mice were genotyped using the following PCR conditions: forward primer: 5′-GCAGCCAAACAGATTACACC-3′ and reverse primer: 5′-AGCAGCCAGCACGGACTACT-3′ for 35 cycles of 95°C for 1 min, 65°C for 1 min, 72°C for 1.5 min. Because the primers flanked one of the loxP sites, these conditions yielded one of three products: an amplified 700 bp fragment corresponding to the WT allele which is included as an illustrative control, a 400 bp fragment corresponding to the KO allele, and an 850 bp fragment corresponding to a floxed allele. Floxed mice were used as controls for all experiments.

Sleeping beauty (SB) vectors encoding the mutant forms of β-catenin and Yes-associated protein (YAP) (11,17) were introduced via hydrodynamic tail vein injection (HDTVI) into 7–8 week-old wild type and pKO mice as previously described (11,12). An additional group of *Pdha1*-floxed mice (control mice) were injected with a Cre recombinase-encoding SB vector in addition to β-catenin and YAP plasmids to produce a tumor-restricted KO of PDC (rKO) (Fig. 1 A–B). Tumor-baring mice were euthanized when tumor burdens caused obvious physical distress. At the time of sacrifice, livers or tumors were divided into small pieces, snap-frozen in liquid nitrogen, and stored at −80C until further analyzed.

FRG-NOD *fah* −/− mice, used as recipients for hepatocyte transplants (Yecuris, Inc., Tualatin, OR), were bred and maintained on 8 mg/L of 2-(2-nitro-4-

Author Manuscript Author Manuscript Author Manuscript Author Manuscript

trifluoromethylbenzoyl)-1,3-cyclohexanedione (NTBC, Yecuris) in the drinking water as previously described (14).

Hepatocyte isolation, transplantation and evaluation

Hepatocytes were isolated using a two-step collagenase perfusion method as previously described (14,18). Briefly, after induction of general anesthesia, a catheter was inserted into the portal vein or inferior vena cava and 0.3 mg/ml of a collagenase II solution (Worthington Biochemical Corp, Lakewood, NJ) was injected into the liver. Digested livers were then removed and incubated in DMEM-F12 with 15 mM HEPES (Corning, Inc. Corning NY) + 5% FBS, passed through a 70 μm cell strainer and centrifuged at 55 × g for 3 min to remove large fragments and non-parenchymal cells. Following two washings, hepatocyte viability was determined by trypan blue exclusion. Only isolates with viabilities exceeding 80% were processed further. Control and KO hepatocytes were then combined and 1.5×10^5 of each was injected directly into the spleens of 6–8 week-old recipient FRG-NOD mice as previously described (14,18) (Fig. 2A). Mice were subsequently maintained under standard conditions with the inclusion of NTBC in their drinking water. Two weeks after transplantation, NTBC was discontinued until mice showed a weight loss of >20% of body weight compared to age-matched controls, at which point NTBC was re-started. Upon regaining the lost weight, NTBC was again discontinued and such cycling was maintained until stable body weights were achieved (generally about 10–12 weeks). Mice were then maintained under NTBC-free conditions for an additional 4–5 wks to ensure maximal hepatic parenchymal replacement by donor hepatocytes. Hepatocytes were then isolated as described above except that the collagenase II concentration was increased to 1 mg/ml. Isolated hepatocytes were washed and snap frozen in small aliquots for subsequent PCR-based analysis to evaluate reconstitution.

The assessment of the hepatocyte composition of transplant recipients was performed by a two-step TaqMan-based PCR (Fig. 2B–D and Supplementary Fig. S1 A–C). Each PCR reaction was performed using the Kapa Probe Fast qPCR kit (Kapa Biosystems, Wilmington, MA) in a total volume of 12 μl containing 10 ng of input genomic DNA. The conditions for amplification were 95°C for 10 sec, 40 cycles at 95°C for 15 sec, 60°C for 60 sec. The total repopulation percentage was determined as described by using the primers that amplified the Pol2neo cassette region inserted into exon 5 of the *fah*−/− mice (forward: 5′-GGGAGGATTGGGAAGACAATAG-3′, reverse 5′-ATTCTCCTTGCCTCTGAACATAA-3′). The product was detected in real time with the probe: 5′/56-FAM/CTTCTGAGG/ZEN/CGGAAAGAA/3IABkFQ/-3′. A standard curve containing known percentages of *fah*−/− and *fah+/+* hepatocytes was created in parallel to allow a determination of the fractional composition of the transplanted samples (Supplementary Fig. S1A). The fractional contribution of control and KO hepatocytes was then determined using two additional primer pairs: the first amplified a region flanking the loxP site within the control population (forward: 5′-CCACACTGTGCAAACCTATTTC-3′, reverse: 5′CTGAAGAGGAGTTTACGTCCAG-3′ (with partial homology to the loxP site) and detected with the probe: 5′-/56-FAM/ATTCCACTC/ZEN/TCCAGCACC/3IABkFQ/-3′), while the second reaction amplified a portion of the cre cassette within the KO population based on the Jackson Laboratories genotyping protocol (forward: 5′-

Author Manuscript Author Manuscript Author Manuscript Author Manuscript

GCGGTCTGGCAGTAAAAACTATC-3′, reverse: 5′-GTGAAACAGCATTGCTGTCACTT-3′, and detected with the probe: 5′/56-FAM/AAACATGCT/ZEN/TCATCGTCGGTCCGG/3IABkFQ/-3′). A standard curve was again created with known amount of control and KO DNA combined to which the unknown samples could be compared (Supplementary Fig. S1 B–C). All ΔCt values were compared to a positive internal control that amplified a 73-bp product of the nuclear apolipoprotein B gene (forward: 5′-CAC GTG GGC TCC AGC ATT-3′, reverse: 5′-TCACCAGTCATTTCTGCCTTTG-3′, amplified with the probe 5′/Cy5-CCAATGGTCGGGCACTGCTCAA/3IABkFQ/–3′). All primers and probes were synthesized by IDT, Inc. (Coralville, IA). PCR reactions were performed on a CFX96 TouchTM Real-Time PCR Detection System (Bio-Rad, Inc.).

Metabolic studies

Immunoblotting, BNGE, mitochondrial DNA quantification, electron transport chain activity assessment, and all metabolic assays were performed as previously described. (12,14,19).

Immuno-blotting

Tissues were prepared for immuno-blotting by lysing in SDS-lysis buffer containing protease, kinase and phosphatase inhibitors as previously described (14). All samples were prepared once and run in the same order for all blots within each group; a loading control was run in all instances where this was possible to again assure sample concentrations were equal. Immunoblots were developed using SuperSignal™ West Pico Chemiluminescent Substrate kit (Thermo Fisher, Waltham, MA). A list of all antibodies, the vendors from which they were obtained and the conditions used is provided in Supplementary Table S1.

Electron transport chain activity

All Oxphos determinations were performed on an Oroboros Oxygraph 2k instrument (Oroboros Instruments, Inc., Innsbruck, Austria) as previously described (12,14). Briefly, ~50 mg of tissue was disrupted on ice in MiR05 buffer (110 mM sucrose; 3 mM $MgCl_2$; 0.5 mM EGTA; 60 mM potassium lactobionate; 20 mM taurine; 10 mM KH_2PO_4; 20 mM HEPES, pH 7.2; and 1 mg/ml fatty acid-free BSA). O_2 consumption rates were quantified in 2 ml of Mir05 buffer containing 10 μM cytochrome *c* and ~40 μg of tissue lysate, 5 mM (final concentration) pyruvate, 5 mM malate, 5 mM ADP and 10 mM glutamate were then sequentially added to initiate electron flow. After achieving the plateau O_2 consumption rate, 10 mM succinate was added to determine the total activities of Complex I + II. Rotenone (0.5 μM) was then added to inhibit Complex I and allow an assessment of Complex II activity. All activities were then normalized to total protein.

Blue native gel electrophoresis (BNGE) and in situ enzymatic assays

BNGE and *in situ* enzymatic assays of ETC complexes were performed as described previously (19). Complexes were electrophoresed on a 3–12% gradient Native PAGE Novex Bis-Tris gels (Invitrogen, Inc., Carlsbad, CA), and stained with Bio-Safe Coomassie G250 (Bio-Rad, Hercules, CA, USA). *In situ* assays were performed for Complex I (NADH ubiquinone oxidoreductase), Complex III (decylubiquinol cytochrome c oxidoreductase),

Author Manuscript Author Manuscript Author Manuscript Author Manuscript

Complex IV (cytochrome c oxidase) and Complex V (ATPase) as previously described (19). Complex II (CII) (succinate dehydrogenase) measurements were performed *in vitro* on total mitochondrial lysates (19).

PDC, FAO, acetate incorporation, ATP and citrate synthase assays

PDC and FAO assays were performed on fresh liver and tumors as previously described (12). Briefly, PDC assay used 50–80 mg of minced tissue in glucose-, glutamine-, and pyruvate-lacking DMEM that was then placed in 0.5 μl aliquots into 0.5 ml of 2× assay buffer containing 0.15 μCi [1-^{14}C]-labeled pyruvate (7.64 mCi/mmol, Perkin Elmer). Reactions were performed in sealed tubes with a central hanging basket (Kimble-Chase Life Science and Research Products, Rockwood, TN) containing a glass microfiber filter (Whatman/GE Healthcare) soaked in 0.5M KOH. Reactions were incubated at 37°C and terminated by adding 0.5 ml of 4.0M perchloric acid. The released $^{14}CO_2$ was then collected on filters for 40 min at 37°C and quantified by scintillation counting.

Fatty acid oxidation (FAO) assays used ~50 mg tissue minced in SET buffer that was then homogenized by five passes in a Potter-Elvehjem homogenizer on ice; 5 μL was then added to 195 μl of the reaction mixture (containing 100mM sucrose, 10mM Tris-HCl, 5mM KH_2PO_4, 0.2mM EDTA, 80mM KCl, 1mM $MgCl_2$, 2mM L-carnitine, 0.1mM malate, 0.05mM coenzyme A, 2mM ATP, 1mM DTT, 0.3% fatty acid-free BSA, pH 8.0) and 0.5 uCi per ml (125 uM final fatty acid concentration) ^{3}H-labeled BSA-conjugated palmitate (Perkin Elmer). Reactions were incubated at 37°C and stopped with the addition of 40 μl 1M KOH, then incubated at 60°C after which perchloric acid was added. Organic extraction was then performed and the water-soluble products of FAO (^3H_2O) were measured by scintillation counting.

Acetate conversion assays were performed on fresh tissue. Approximately 40–50 mg of tissue was finely minced small pieces in 200 μl of 2x reaction buffer (containing 100mM sucrose, 10mM Tris-HCl, 5mM KH_2PO_4, 0.2mM EDTA, 80mM KCl, 1mM $MgCl_2$, 2mM L-carnitine, 0.1mM malate, 0.05mM coenzyme A, 2mM ATP, 1mM DTT, 0.3% fatty acid-free BSA, pH 8.0), 0.4 μl 1M sodium acetate, 2.5 μl 20% glucose, 196.6 μl PBS, and 0.5 μl of ^{3}H-labeled acetate (1.59 Ci/mmol, Perkin Elmer), which was then incubated at 37°C for 4 h. Samples were placed on ice to stop the reaction and tissue pieces were washed three times with 400 μl aliquots of cold phosphate-buffered saline (PBS). Samples were homogenized using a bullet blender in 400 μl cold PBS. Organic extraction was performed in chloroform following the protocol of Bligh and Dyer (20) and lipid-soluble products were measured by scintillation counting.

ATP assays were performed on lysates of previously snap-frozen tissue using the ATP Lite ATP detection system (Perkin-Elmer, Inc. Downers Grove, IL). Instructions from the manufacturer were followed and each point was performed in triplicate and normalized to protein.

Citrate synthase assays were performed on isolates of previously snap-frozen tissue using the protocol described by Oroboros Instruments, Inc. (http://wiki.oroboros.at/images/4/40/MiPNet17.04_CitrateSynthase.pdf). Briefly, homogenized liver samples were diluted in

Author Manuscript Author Manuscript Author Manuscript Author Manuscript

Tris-HCl buffer (0.1 M, pH 7.1) in a concentration of 1–2mg/mL, and 5 μL of the sample was added to a master mix containing 5 μL 12.2 mL acetyl-CoA in water, 5 μL 10% Triton X-100 in water, 20 μL 1.01 mM DTNB in 1M Tris-HCl pH 8.0, and 155 μL water in a 96-well plate. Oxaloacetate was added to Triethanolamine-HCl buffer (0.1 M, pH 8.0) for a final concentration of 10 mM, pH 8.0. Oxaloacetate solution (10 μL of 10mM solution) was then added to the sample in the master mix to start the reaction. Fluorescence was measured at 420 nm for 120 s using a plate reader (FLUOstar Omega, BMG Labtech) and compared to a standard curve generated with known amounts of enzyme.

Mitochondrial DNA (mtDNA) quantification

Mitochondrial DNA was quantified using a previously described protocol (12). Briefly, PCR primers were designed to amplify a portion of the cytochrome c oxidase I gene using the TaqMan based approach. Products were normalized to a similar-sized product of the apolipoprotein B gene. All primers and probes were synthesized by IDT, Inc. (Coralville, IA).

Blood lactate assays

Whole blood was obtained from mice prior to euthanasia by creating a small nick in the tail with a razor blade. Free flowing blood was then captured by the sensor and immediately analyzed by the Lactate Scout+ meter (SensLab EKF Diagnostics, Leipzig, Germany).

Mass spectroscopy

Extraction of metabolites—Liver and tumor tissues were homogenized by adding 1 mL of 80% methanol in a vial containing lysing matrix D (MP Biomedicals, Salon, Ohio) and using a high-speed bench-top homogenizer (Fastprep, MP Biomedicals) for 2 min. The homogenates were incubated on ice for 30 min before adding 0.25 mL of chloroform and repeating the homogenization. The upper polar phase was separated after centrifugation and used for further analysis. Similar extraction was also performed for ^{13}C algal cells (Sigma-Aldrich, St. Louis, MO) that were used as an internal standard for metabolites.

LC-MS analysis of organic acids—Organic acids were analyzed by derivatizing them to their corresponding 3-nitrophenylhydrazones (21). Briefly 100 μL of the supernatant was heated at 50°C with 50 μL of 200 mM 3-nitrophenylhydrazine in 50% aqueous acetonitrile and 50 μL of 120 mM N-(3-dimethylaminopropyl)-N′-ethylcarbodiimide HCl in a 6% pyridine solution in the same solvent for 20 min. 100 μL of the mixture was diluted to 500 μL using 50% aqueous acetonitrile (ACN) and 10 μL was injected into the LC-MS Instrument. An Ultimate 3000 RSLC system connected to a Thermo Fisher Scientific Q Exactive mass spectrometer (both from Thermo Fisher Scientific, Waltham, MA) was used for analysis. Reverse phase chromatographic separation was performed on a Phenomenex Luna C18 column (2.1 mm×150 mm, 5 μm) column (Torrence, CA) using gradient elution with a mobile phase comprised of H_2O + 0.1% formic acid (A) and acetonitrile (B), delivered at a flow rate of 0.2 mL/min. The gradient program was 3% B (0–3 min), from 3% B to 95% B (3–50 min), 95% B (50–55 min), from 95% B to 3% B (55–57 min) and 3% B (57–60 min). The mass spectrometer was equipped with an ESI source and was operated in

Author Manuscript Author Manuscript Author Manuscript Author Manuscript

negative mode using a full scan range of 150 *m/z* to 900 *m/z*. Analyte identification was confirmed by high resolution accurate mass and compared to the ^{13}C internal standard.

LC-MS analysis of primary metabolites—The primary polar phase metabolites were separated by ion-pairing reversed phase chromatography on the LC-MS system described above (22). The mobile phase contained 5mM hexylamine in H_2O (A) 5mM hexylamine in acetonitrile (B) delivered at a flow rate of 0.15 mL/min with a post column addition of 0.1 mL/min acetonitrile before entering the mass spectrometer. The gradient program was 3% B (0–3 min), from 3% B to 30% B (3–30 min), 30% B to 95% B (30–55 min), 95% B (55–60 min), 95% B-100% B (60–61 min), 100% B (61–66 min), 100% B-3%B (66–67 min), 3% B (67–70 min). The mass spectrometer was operated in negative mode using a full scan range of 100 *m/z* to 900 *m/z*. Analyte identification was confirmed by high resolution accurate mass and compared to the ^{13}C internal standard.

LC-MS/MS analysis of amino acids—Amino acids were analyzed by derivatizing them to their phenylthiocarbamyl derivatives with phenylisothiocyanate (PITC) (23) followed by LC-MS/MS. The polar phase (100 μL) was dried under nitrogen and dissolved in 100 μL of coupling solution [acetonitrile:pyridine:triethylamine:water (10:5:2:3)] plus 20 μL of PITC and reacted for 15 min at room temperature. The samples were vacuum-dried, dissolved in 200 μL of 50% acetonitrile and 10 μL was injected into a Shimadzu/CTC PAL HPLC coupled to a Sciex 6500 QTrap (Framingham, MA) for analysis. Reversed phase separation was performed on a Phenomenex C18 Luna column as described above using a gradient elution with a mobile phase consisting of 0.1% acetic acid in H_2O (A) and 0.1% acetic acid in acetonitrile (B), delivered at a flow rate of 0.4 mL/min. The gradient program was 3% B (0–3 min), 3% B to 100% B (3–20 min), 100% B (20–25 min), 100% B to 3% B (25–26 min), 3% B (26–30 min). The mass spectrometer was equipped with an ESI turbo V ion source that was operated in the positive mode using scheduled multiple reaction monitoring. Analyte peak areas were normalized to their corresponding ^{13}C internal standard.

Statistical analysis

For statistical evaluation, GraphPad Prism 6 (GraphPad Software, Inc.) was used. One-way ANOVA with Tukey's multiple comparisons was employed; if groups had unequal variance (determined by the Brown-Forsythe test), data were log-transformed for analysis. Survival curves were compared with Mantel-Cox log-rank tests. All error bars, unless otherwise noted, are mean +/- SEM.

Results

Control and KO hepatocytes regenerate equally well

Mice lacking the enzyme fumaryl acetoacetate hydrolase (FAH) mimic type I hereditary tyrosinemia and succumb to the accumulation of cytotoxic tyrosine catabolites (14,18) unless rescued with the drug 2-(2-nitro-4-trifluoro-methyl-benzoyl)-1,3-cyclo-hexanedione (NTBC), which blocks the enzyme p-hydroxyphenylpyruvate dioxygenase (HPD) that lies upstream of FAH. A 'genetic' cure can also be achieved by transplanting as few as 10^5 *fah +/+* hepatocytes, which eventually partially replace the diseased hepatic parenchyma. Mixed

Author Manuscript Author Manuscript Author Manuscript Author Manuscript

donor hepatocyte populations afford an even more sensitive means of assessing even small differences in long-term repopulation potential (14).

Approximately equal numbers of *fah*+/+ control (*Pdha1*-floxed) and *Pdha1*-KO (KO) hepatocytes were mixed and inoculated intra-splenically into recipient (*fah*−/−) *FRG-NOD* mice (14,15). Eventual discontinuation of NTBC was then carried out over the next 10–12 wks (14) followed by an additional 4–5 wks of NTBC-independent recovery (12). As seen in Fig. 2E, total donor hepatocytes comprised 65–83% (mean 76%) of the entire liver population after transplantation. The contribution of donor hepatocytes closely matched that of the input inoculum (Fig. 2F), signifying equal repopulation capacity.

Genetic ablation of *Pdha1* minimally affects tumorigenesis

In a model of HB induced by the over-expression of mutant β-catenin and YAP, the survival of tumor-bearing control and pKO mice was nearly identical, whereas the survival of rKO mice was modestly prolonged (Fig. 3A). This was not attributable to differences in *Pdha1* gene excision efficiency (Fig. 3B) or levels of tumor-associated PDHα protein (Fig. 3C and D). PDC enzyme activity was higher in control livers versus pKO livers, and increased by 3–4 fold in control tumors, as seen previously (12). In contrast, PDC activity did not increase in pKO or rKO tumors over the KO liver (Fig. 3E). Control HBs also expressed less phosphorylated, inactive PDHα, less inhibitory PDK1 and more PDP2 (Fig. 3C and D) (7). Interestingly, despite the lack of PDC in pKO and rKO tumors, the behavior of both PDK1 and PDP2 closely mimicked that of control HBs. Thus, the differential survival of HB-bearing pKO and rKO mice was not attributable to altered levels of PDH protein, PDC activity or its key up-stream regulators.

Despite the similar survival of tumor-bearing control and pKO mice (Fig. 3A), HBs from the latter group were on average ~20% smaller (Fig. 3F), whereas rKO tumor sizes were similarly sized. An explanation for these findings was provided by the observation that blood lactate levels of tumor-bearing pKO mice prior to sacrifice were significantly higher than those of either tumor-bearing control or rKO mice (Fig. 3G). This suggested that excessive lactate production and the accompanying metabolic acidosis contributes to the premature demise of tumor-bearing pKO mice, whereas the lactate produced by pKO tumors is metabolized by the surrounding PDC-replete liver parenchyma, thus preventing acidosis and allowing the tumors to achieve a larger size. Large pKO tumors also likely restrict diaphragmatic excursion and thus contribute to the underlying acidosis of pKO mice by limiting respiratory compensation.

Finally, we assessed PDHα and pPDHα by immunohistochemistry in a small number of primary human HBs, with typical results shown in Fig. 3H. A subset of six HBs, comprised primarily of those with well-differentiated fetal histology, showed lower levels of pPDHα staining (0–1+) than was seen in eleven tumors with crowded fetal histology (2–3+).

PDC deficient tumors efficiently conduct Oxphos despite AcCoA depletion

As demonstrated previously (12,14), Complex II was the most important contributor to the ETC in all tissues (Fig. 4A), though its activity was reduced by 40–50% in tumors. Although Complex I contributed minimally to overall ETC function, its activity was higher in control

Author Manuscript Author Manuscript Author Manuscript Author Manuscript

tumors than in control livers whereas this was not the case with pKO livers and tumors and likely reflected the inability of these tissues to furnish AcCoA when supplied with exogenous pyruvate. Overall, oxygen consumption was decreased in all tumors, regardless of genotypes (Fig. 4A). Although control HBs were associated with a significant loss of mitochondrial mass, thus at least partially explaining the Warburg effect (12), this finding was less pronounced in KO tumors (Fig. 4B).

To investigate potential alternative sources of AcCoA in KO tumors, we examined fatty acid utilization. Compared to normal livers, WT HBs are less reliant on long-chain fatty acid β-oxidation (FAO) as an energy source probably because, in rapidly dividing tumor cells, the fatty acids are used directly for the *de novo* synthesis of membrane lipids (12). Again, FAO in control, pKO and rKO HBs was markedly reduced relative to their corresponding livers (Fig. 4C). Thus, increased FAO did not appear to supply the mitochondrial AcCoA needed to compensate for the lack of glucose-derived pyruvate.

Mostly derived from the gut microbiome (24), acetate is converted to AcCoA via mitochondrial AcCoA (acyl CoA) synthetase 1 (25). This can be assessed indirectly by monitoring the conversion of ^{3}H-acetate into lipids via the sequential conversion of acetate-derived mitochondrial AcCoA into citrate by citrate synthase, the cytoplasmic re-derivation of AcCoA from citrate by ATP citrate lyase, and the incorporation of the ^{3}H label into fatty acids and steroids by fatty acid synthase and HMG coenzyme A reductase, respectively (26). We found no differences among any of the cohorts, suggesting that KO tumors did not increase their conversion of acetate to AcCoA to compensate for the loss of PDC activity (Fig. 4D). Finally, in an assay that measured $^{14}CO_2$ release from ^{14}C-leucine, we were unable to show evidence for up-regulation of branched-chain amino acid oxidation as a source of AcCoA (not shown).

Lacking evidence that PDC loss was accompanied by compensatory increases in AcCoA production from any of the above-discussed alternative non-glycolytic sources, we measured the actual steady state levels of AcCoA by mass spectroscopy (MS) and found them to be highly depleted in both KO livers and HBs (Fig. 4E).

Finally, we measured ATP levels in each of the tissues. As seen in Fig. 4F and as previously reported (12), control tumors contained higher levels of ATP than control livers. Although the ATP levels of KO livers were equivalent to those in control livers, no increases were observed following transformation.

Control and KO tissues possess similar ETC structure and function but different levels of metabolic intermediates

Despite their failure to oxidize pyruvate, their attenuated Complex II activity and their depleted AcCoA content, both KO livers and tumors showed identical patterns of ETC complex structure as determined by blue native gel electrophoresis (Supplementary Fig. S2A) and closely paralleled their control counterparts (Supplementary Fig. S2 B–G). Thus, the basic ETC structure and its enzymatic activities remain largely intact in KO animals.

Author Manuscript Author Manuscript Author Manuscript Author Manuscript

A comparative MS analysis of TCA cycle intermediate levels among the four tissue groups using MS (Fig. 5A and Supplementary Fig. S3) revealed marked differences between control and KO tissues in addition to the afore-mentioned AcCoA depletion (Fig. 4E). For example, relative to control livers, KO livers showed comparable levels of citrate and iso-citrate but tended to contain lower levels of all other measureable intermediates, notably α-ketoglutarate and malate. Relative to control tumors, KO tumors had decreased levels of isocitrate, fumarate and malate and NAD+; in contrast, the levels of most TCA intermediates in KO tumors were little changed relative to those in KO livers.

TCA substrate normalization in KO tissues could occur by compensatory mechanisms, including increased glutaminolysis (2,27). However, the expression of key enzymes involved in the conversion of glutamine to α-ketoglutarate, including glutamate dehydrogenase 1/2, and particularly the rate-limiting, liver-specific enzyme glutaminase 2 (Gls2), were down-regulated in both control and KO tumors (Fig. 5B). Similarly, citrate synthase (CS) catalyzes the condensation of AcCoA and oxaloacetate to furnish citrate, which can then be utilized as either a TCA cycle intermediate or a substrate for the extra-mitochondrial fatty acid synthesis (28,29). We therefore directly measured CS activity; although control HBs demonstrated this expected increase in activity, so too did both KO livers and tumors (Fig. 5C).

MS analyses of select glycolytic pathway intermediates showed fewer differences in KO tumors compared to control, with the exception of lower levels of phosphoenolpyruvate (Supplementary Fig. S4 and Supplementary Fig. S5).

Complex alterations in intracellular amino acid levels occur in both control and KO tissues

Another potential source of TCA cycle intermediates is from the oxidation of amino acids, all of which except lysine can be directly catabolized to one of six TCA intermediates. Indeed, even lysine itself can contribute indirectly via the conversion of its end product acetoacetyl CoA to AcCoA (30). We were able to quantify 17 amino acids in each of the above tissues and found only modest alterations in their steady-state levels (Fig. 6 and Supplementary Fig. S6). Compared to control livers, control tumors contained increased levels of threonine and decreased level of alanine. While KO tumors demonstrated a similar increase in threonine levels, they had an increase in alanine compared to control tumors.

Discussion

Although rapidly proliferating cells are highly reliant on glycolysis as an energy source, the up-regulation of PDC activity that we have observed in HBs (Fig. 3C–E) (12) suggests that these tumors require a combination of glycolysis and the TCA cycle to support both energetic and anabolic demands. We have hypothesized that increased PDC activity represents a compensatory attempt to normalize low levels of AcCoA that is aided by the known negative regulation of PDC by AcCoA (6,7,31). An additional metabolic incentive to up-regulate PDC activity may be that tumors have only modestly higher levels of pyruvate than livers (Supplementary Fig. S5), even in the face of an increased need for this substrate to furnish AcCoA for non-mitochondrial functions such as *de novo* fatty acid and sterol biosynthesis. Nonetheless, we found proliferative rates of control and KO hepatocytes to be

Author Manuscript Author Manuscript Author Manuscript Author Manuscript

indistinguishable, and the rates of KO tumor growth to be only modestly impaired. Overall, these results reveal the remarkable ability of PDC-deficient hepatocytes to compensate for the loss of this central metabolic enzymatic complex.

The greater mitochondrial mass of KO tumors (Fig. 4B) may partially explain how they compensate for their lack of pyruvate-derived AcCoA, but raises the question as to what other sources of this substrate might be utilized given its centrality to both oxidative and non-oxidative mitochondrial functions. However, we were unable to document increased utilization of fatty acids, acetate or branched-chain amino acids for these purposes. Although these pathways represent the major secondary means by which mitochondrial AcCoA could be generated, it remains possible that less standard substrates such as cholesterol or a more select group of amino acids such as valine or isoleucine are also utilized for this purpose. However, the markedly reduced AcCoA levels in KO livers and tumors (Fig. 4E) implies that such alternate sources of this intermediate most likely do not exist. Our findings disagree with a recent report showing that KO livers have normal AcCoA levels (32), though that report also did not identify an alternative AcCoA source. This discrepancy most likely relates to the methods for AcCoA detection, i.e. high resolution mass spectrometry, versus an indirect fluorescence-based enzymatic assay that requires sample de-proteination. Overall, we propose that the absence of PDC activity severely depletes the AcCoA pool, which is nonetheless sufficient to support normal or near-normal levels of proliferation. Some additional advantage may derive from an increase in KO tumor mitochondrial mass that may occur in response to the less efficient TCA cycle-derived energy production that accompanies a depletion of AcCoA stores (Fig. 4B, E).

In addition to the profound depletion of AcCoA that we observed, steady-state metabolic profiling (Fig. 5 and Supplementary Fig. S3) revealed several additional metabolic alterations. That KO tumor pyruvate levels did not exceed those in control tumors almost certainly reflects the increased activity of lactate dehydrogenase and the conversion of any excess pyruvate to lactate (Fig. 3G) in a reaction that requires NADH, which is produced in excess by the Warburg effect. PDC loss was also accompanied by an incompletely compensated depletion of several TCA cycle intermediates as might be expected given the low levels of AcCoA (Fig. 4E). Despite this depletion, glutaminolysis does not appear to be increased in either control or KO tumors to provide non-pyruvate-derived TCA substrates and circumvent the metabolic block imposed by PDC's absence (Fig. 5B).

One exception to the depleted TCA cycle intermediates in KO was citrate, the levels of which were equal in all four tissues. This suggests that, at least in the circumstances studied here, the maintenance of normal citrate pools is not necessarily reliant on prevailing AcCoA levels. Alternative ways of maintaining citrate levels (at least within mitochondria) include reducing its transport to the cytoplasm (33) for use in lipid biosynthesis and/or increasing cellular uptake from dietary sources. The first of these possibilities is consistent with our previous suggestion that the synthesis of new membranes to support tumor proliferation may preferentially rely on pre-formed fatty acids and cholesterol rather than on their *de novo* synthesis from citrate (12). Finally, citrate synthase, which catalyzes the formation of citrate from oxaloacetate and AcCoA, is strongly inhibited by AcCoA (34). This is consistent with

Author Manuscript Author Manuscript Author Manuscript Author Manuscript

our findings (Fig. 5C) and suggests that this elevated activity might be sufficient to maintain normal citrate levels in the face of reduced AcCoA stores.

Further consistent with the overall depletion of TCA cycle substrates, both NAD^+ and NADH levels were also reduced in KO livers. NADH depletion was likely further abetted by the loss of production that accompanies pyruvate's conversion to AcCoA. NADH donates electrons to Complex I of the ETC, thus perhaps explaining why Complex I activity did not increase in KO tumors as it did in control tumors (Fig. 4A). Despite these changes, loss of the PDC does not alter intrinsic ETC function (Fig. 4A and Supplementary Fig. S2), indicating that at least some TCA substrates in control tissues are in excess of those needed to support neoplastic proliferation.

An unanswered question concerns the source of reducing equivalents in the mitochondria of KO tumors, whose levels of TCA substrates were not much different than those in KO livers, yet whose NADH levels were considerably higher than their liver counterparts (Fig. 5A and Supplementary Fig. S3). It is possible that these derive from the cytoplasm via the glycerol phosphate shuttle (35) and that the high levels of glycolysis provide sufficient NADH for this purpose. On the other hand, most cytoplasmic NADH is likely oxidized back to NAD^+ during the conversion of pyruvate to lactate. The ultimate contribution of this shuttle to mitochondrial NADH may well depend on the balance between these two competing sets of reactions. Whatever the ultimate source of NADH in KO tumors, it is noteworthy that its levels essentially match those of control tumors despite the depletion of many TCA intermediates (Fig. 5A and Supplementary Fig. S3).

Similarly, though our MS measurements did not quantify FAD or $FADH_2$, respirometry indicated that levels of the latter were sufficient to support the oxidative requirements of KO tumors despite the ~50% reduction of succinate and fumarate levels (Fig. 4A and Supplementary Fig. S3). Indeed, the overall activity of Complex II was equivalent in control and KO tumors. The succinate dehydrogenase (SDH) activity in KO tumors as measured by direct *in situ* enzymatic assay did tend to be somewhat higher, potentially suggesting an increased rate of catalytic activity to compensate for the lack of substrate (Supplementary Fig. S2G). On the other hand, the overall increase in KO tumor mitochondrial mass (Fig. 4B) might be sufficient to provide for control tumor levels of Complex II respiration despite their overall substrate deficit.

Taken together, the foregoing studies support the idea that neither the steady-state levels of TCA substrates nor Oxphos are entirely dependent on AcCoA supply. Rather, multiple points of entry for non-TCA cycle intermediates may allow for the generation of both substrates and reducing equivalents in a manner that is at least partially AcCoA-independent. That O_2 consumption in response to succinate proceeded equally well in control and KO tissues (Fig. 4A) further suggests that the normal circularity of the TCA cycle is also not necessarily mandatory. This implies that respiration can sometimes proceed in a linear manner and in the absence of AcCoA generation from any extra-mitochondrial source simply by supplying succinate.

Author Manuscript Author Manuscript Author Manuscript Author Manuscript

However, the non-circular directionality of the TCA cycle may also prove somewhat of an energetic disadvantage as evidenced by the low ATP levels in KO tissues (Fig. 4F). The lack of NADH from the conversion of pyruvate to AcCoA likely also contributes to the paucity of ATP in the KO tumors. Nonetheless, the consequences of this appear to be rather minimal, especially on tumor growth rates (Fig. 3A). The high ATP levels in control tumors may therefore simply be a bi-product of the significant up-regulation of glycolysis for anabolic purposes, rather than being a true proliferative necessity.

A recent report has suggested that, at least *in vitro* and in the presence of high oxygen and exogenous nutrient concentrations, the suppression of the PDC only minimally affected the growth of murine embryonic fibroblasts and H460 lung cancer cells. These cells derived the majority of their AcCoA from extracellular lipids and utilized reductive carboxylation of glutamine to drive fatty acid synthesis (36). However, kinetic labeling experiments showed that, despite a ca. 90% loss of PDC activity, 30–50% of ^{13}C-labeled glucose was still incorporated into citrate within 4 hr. This suggests that residual PDC activity might have contributed to the relatively mild phenotype of these cells to a greater degree than indicated by enzymatic assay. However, FAO not only inhibits glycolysis, but is also a less efficient form of energy production that generates high levels of genotoxic reactive oxygen species (37–39). Furthermore, unlike the conversion of pyruvate to AcCoA, FAO does not furnish NADH. These studies suggest that tumors with an excessive reliance on FAO might be at a proliferative disadvantage relative to those in which AcCoA derived from pyruvate. At the same time, they emphasize the heterogeneity of metabolic regulation that can be found among different tumors and how this can vary under different conditions.

Several studies have demonstrated changes in PDC activity in cancer that are contrary to those presented here. For example, some tumor cells cultured *in vitro* under ambient oxygen concentrations down-regulate PDH, thereby suggesting that, analogous to the case of the M2 isoform of pyruvate kinase (3), low PDH activity facilitates the accumulation of upstream glycolytic intermediates for biosynthetic purposes (40,41). Similarly, dichloroacetate-mediated inhibition of PDK1 and the accompanying increase in PDC impairs the growth of certain tumors (42–44). In contrast, and in keeping with our results, some cancers express high levels of PDC activity suggesting that glucose simultaneously supplies both AcCoA and metabolic intermediates (45–48). Indeed, the enforced expression of c-Myc (Myc), an oncoprotein that is deregulated in a majority of human cancers (49), increases both glycolysis and oxidative phosphorylation (Oxphos) in non-transformed fibroblasts when oxygen is plentiful, significantly increasing mitochondrial mass and growth rates (50,51). Under similar conditions, ~50% of AcCoA that is incorporated into fatty acids and acetyl lysine residues in nuclear histones derives from glucose (52). Thus, PDC's role in supporting cancer cell growth is variable and subject to multiple inter-dependent factors including cell type, the nature of the transforming signals, nutrient and oxygen availability and the cell's actual replicative and metabolic status. In the case of tumors such as those studied here, where maintaining high levels of PDH activity appears to be essential for generating normal levels of AcCoA, it is tempting to speculate that this enzyme complex might represent an actionable therapeutic target. On the other hand, it seems likely that such an approach may prove problematic given the likelihood that extremely efficient enzymatic

Author Manuscript Author Manuscript Author Manuscript Author Manuscript

inhibition is likely to be necessary to significantly inhibit tumor growth and is also likely to be associated with significant lactic acidosis.

In summary, we show that glycolysis and the TCA cycle can be dissociated from one another by the targeted inactivation of the *Pdha1* gene without affecting the normal proliferative capacity of hepatocytes and only modestly impairing their neoplastic growth. *Pdha1* inactivation leads to significant metabolic re-programming as evidenced by complex changes in the steady-state levels of glycolytic intermediates, TCA cycle substrates and amino acids. Despite these adaptations, AcCoA levels remain extremely low yet sufficient to support proliferative, biosynthetic and energetic demands. Potential compensatory sources of AcCoA could not be clearly identified, suggesting that any one of these contributes only minimally at best to the steady-state pool and that any resultant inefficiencies in mitochondrial energy or TCA substrate production may be offset by increases in mitochondrial mass. Thus, whether relying on oxidative or non-oxidative modes of respiration, hepatocytes can still balance the energy and metabolic contributions of these two pathways despite the severing of their direct metabolic bridge.

Supplementary Material

Refer to Web version on PubMed Central for supplementary material.

Acknowledgments

Financial support: L.E. Jackson was supported in part by NIH/NICHD T32 training grant HD071834-04. J.M. Dolezal was supported in part by the Clinical Scientist Training Program at the University of Pittsburgh School of Medicine. The work was also supported by NIH RO1 grant CA174713 awarded to E.V. Prochownik, and by NIH RO1 grant DK103645 awarded to A.W. Duncan.

References

1. Wellen KE, Thompson CB. A two-way street: reciprocal regulation of metabolism and signalling. Nature reviews Molecular cell biology. 2012; 13:270–6. [PubMed: 22395772]
2. Stine ZE, Dang CV. Stress eating and tuning out: cancer cells re-wire metabolism to counter stress. Critical reviews in biochemistry and molecular biology. 2013; 48:609–19. [PubMed: 24099138]
3. Vander Heiden MG, Cantley LC, Thompson CB. Understanding the Warburg effect: the metabolic requirements of cell proliferation. Science (New York, NY). 2009; 324:1029–33.
4. Brahimi-Horn MC, Bellot G, Pouyssegur J. Hypoxia and energetic tumour metabolism. Current opinion in genetics & development. 2011; 21:67–72. [PubMed: 21074987]
5. Khramtsov VV, Gillies RJ. Janus-faced tumor microenvironment and redox. Antioxidants & redox signaling. 2014; 21:723–9. [PubMed: 24512276]
6. Gray LR, Tompkins SC, Taylor EB. Regulation of pyruvate metabolism and human disease. Cellular and molecular life sciences: CMLS. 2014; 71:2577–604. [PubMed: 24363178]
7. Patel MS, Korotchkina LG. Regulation of the pyruvate dehydrogenase complex. Biochemical Society transactions. 2006; 34:217–22. [PubMed: 16545080]
8. Johnson MT, Mahmood S, Hyatt SL, Yang HS, Soloway PD, Hanson RW, et al. Inactivation of the murine pyruvate dehydrogenase (Pdha1) gene and its effect on early embryonic development. Molecular genetics and metabolism. 2001; 74:293–302. [PubMed: 11708858]
9. Lissens W, De Meirleir L, Seneca S, Liebaers I, Brown GK, Brown RM, et al. Mutations in the X-linked pyruvate dehydrogenase (E1) alpha subunit gene (PDHA1) in patients with a pyruvate dehydrogenase complex deficiency. Human mutation. 2000; 15:209–19. [PubMed: 10679936]

Author Manuscript Author Manuscript Author Manuscript Author Manuscript

10. Choi CS, Ghoshal P, Srinivasan M, Kim S, Cline G, Patel MS. Liver-specific pyruvate dehydrogenase complex deficiency upregulates lipogenesis in adipose tissue and improves peripheral insulin sensitivity. Lipids. 2010; 45:987–95. [PubMed: 20835892]
11. Tao J, Calvisi DF, Ranganathan S, Cigliano A, Zhou L, Singh S, et al. Activation of beta-catenin and Yap1 in human hepatoblastoma and induction of hepatocarcinogenesis in mice. Gastroenterology. 2014; 147:690–701. [PubMed: 24837480]
12. Wang H, Lu J, Edmunds LR, Kulkarni S, Dolezal J, Tao J, et al. Coordinated Activities of Multiple Myc-dependent and Myc-independent Biosynthetic Pathways in Hepatoblastoma. The Journal of biological chemistry. 2016; 291:26241–51. [PubMed: 27738108]
13. Dolezal JM, Wang H, Kulkarni S, Jackson L, Lu J, Ranganathan S, et al. Sequential Adaptive Changes in a c-Myc-Driven Model of Hepatocellular Carcinoma. The Journal of biological chemistry. 2017
14. Edmunds LR, Otero PA, Sharma L, D'Souza S, Dolezal JM, David S, et al. Abnormal lipid processing but normal long-term repopulation potential of myc−/− hepatocytes. Oncotarget. 2016; 7:30379–95. [PubMed: 27105497]
15. Overturf K, Al-Dhalimy M, Tanguay R, Brantly M, Ou CN, Finegold M, et al. Hepatocytes corrected by gene therapy are selected in vivo in a murine model of hereditary tyrosinaemia type I. Nature genetics. 1996; 12:266–73. [PubMed: 8589717]
16. Michalopoulos GK. Liver regeneration after partial hepatectomy: critical analysis of mechanistic dilemmas. The American journal of pathology. 2010; 176:2–13. [PubMed: 20019184]
17. Chen X, Calvisi DF. Hydrodynamic transfection for generation of novel mouse models for liver cancer research. The American journal of pathology. 2014; 184:912–23. [PubMed: 24480331]
18. Duncan AW, Hickey RD, Paulk NK, Culberson AJ, Olson SB, Finegold MJ, et al. Ploidy reductions in murine fusion-derived hepatocytes. PLoS genetics. 2009; 5:e1000385. [PubMed: 19229314]
19. Edmunds LR, Sharma L, Wang H, Kang A, d'Souza S, Lu J, et al. c-Myc and AMPK Control Cellular Energy Levels by Cooperatively Regulating Mitochondrial Structure and Function. PloS one. 2015; 10:e0134049. [PubMed: 26230505]
20. Bligh EG, Dyer WJ. A rapid method of total lipid extraction and purification. Canadian journal of biochemistry and physiology. 1959; 37:911–7. [PubMed: 13671378]
21. Han J, Gagnon S, Eckle T, Borchers CH. Metabolomic analysis of key central carbon metabolism carboxylic acids as their 3-nitrophenylhydrazones by UPLC/ESI-MS. Electrophoresis. 2013; 34:2891–900. [PubMed: 23580203]
22. Coulier L, Bas R, Jespersen S, Verheij E, van der Werf MJ, Hankemeier T. Simultaneous quantitative analysis of metabolites using ion-pair liquid chromatography-electrospray ionization mass spectrometry. Analytical chemistry. 2006; 78:6573–82. [PubMed: 16970336]
23. Ebert RF. Amino acid analysis by HPLC: optimized conditions for chromatography of phenylthiocarbamyl derivatives. Analytical biochemistry. 1986; 154:431–5. [PubMed: 3728962]
24. Bienenstock J, Kunze W, Forsythe P. Microbiota and the gut-brain axis. Nutrition reviews. 2015; 73(Suppl 1):28–31. [PubMed: 26175487]
25. Ikeda Y, Yamamoto J, Okamura M, Fujino T, Takahashi S, Takeuchi K, et al. Transcriptional regulation of the murine acetyl-CoA synthetase 1 gene through multiple clustered binding sites for sterol regulatory element-binding proteins and a single neighboring site for Sp1. The Journal of biological chemistry. 2001; 276:34259–69. [PubMed: 11435428]
26. Hanson RW, Ballard FJ. The relative significance of acetate and glucose as precursors for lipid synthesis in liver and adipose tissue from ruminants. The Biochemical journal. 1967; 105:529–36. [PubMed: 5583995]
27. Altman BJ, Stine ZE, Dang CV. From Krebs to clinic: glutamine metabolism to cancer therapy. Nature reviews Cancer. 2016; 16:619–34. [PubMed: 27492215]
28. Wiegand G, Remington SJ. Citrate synthase: structure, control, and mechanism. Annual review of biophysics and biophysical chemistry. 1986; 15:97–117.
29. Mashima T, Seimiya H, Tsuruo T. De novo fatty-acid synthesis and related pathways as molecular targets for cancer therapy. British journal of cancer. 2009; 100:1369–72. [PubMed: 19352381]

Author Manuscript Author Manuscript Author Manuscript Author Manuscript

30. King, N. Amino Acids and the Mitochondria. In: Schaffer, SW., S, M., editors. Mitochondria: The Dynamic Organelle. New York: Springer; 2007. p. 151-68.
31. Israelsen WJ, Vander Heiden MG. Pyruvate kinase: Function, regulation and role in cancer. Seminars in cell & developmental biology. 2015; 43:43–51. [PubMed: 26277545]
32. Mahmood S, Birkaya B, Rideout TC, Patel MS. Lack of mitochondria-generated acetyl-CoA by pyruvate dehydrogenase complex downregulates gene expression in the hepatic de novo lipogenic pathway. American journal of physiology Endocrinology and metabolism. 2016; 311:E117–27. [PubMed: 27166281]
33. Chappell JB, Robinson BH. Penetration of the mitochondrial membrane by tricarboxylic acid anions. Biochemical Society symposium. 1968; 27:123–33. [PubMed: 4319083]
34. Johansson CJ, Pettersson G. Kinetics of the inhibition of citrate synthase from pig heart by substrate analogues. European journal of biochemistry. 1974; 46:5–11. [PubMed: 4852623]
35. Mracek T, Drahota Z, Houstek J. The function and the role of the mitochondrial glycerol-3-phosphate dehydrogenase in mammalian tissues. Biochimica et biophysica acta. 2013; 1827:401–10. [PubMed: 23220394]
36. Rajagopalan KN, Egnatchik RA, Calvaruso MA, Wasti AT, Padanad MS, Boroughs LK, et al. Metabolic plasticity maintains proliferation in pyruvate dehydrogenase deficient cells. Cancer & metabolism. 2015; 3:7. [PubMed: 26137220]
37. Chambers KT, Leone TC, Sambandam N, Kovacs A, Wagg CS, Lopaschuk GD, et al. Chronic inhibition of pyruvate dehydrogenase in heart triggers an adaptive metabolic response. The Journal of biological chemistry. 2011; 286:11155–62. [PubMed: 21321124]
38. Rosca MG, Vazquez EJ, Chen Q, Kerner J, Kern TS, Hoppel CL. Oxidation of fatty acids is the source of increased mitochondrial reactive oxygen species production in kidney cortical tubules in early diabetes. Diabetes. 2012; 61:2074–83. [PubMed: 22586586]
39. Fillmore N, Mori J, Lopaschuk GD. Mitochondrial fatty acid oxidation alterations in heart failure, ischaemic heart disease and diabetic cardiomyopathy. British journal of pharmacology. 2014; 171:2080–90. [PubMed: 24147975]
40. Hitosugi T, Fan J, Chung TW, Lythgoe K, Wang X, Xie J, et al. Tyrosine phosphorylation of mitochondrial pyruvate dehydrogenase kinase 1 is important for cancer metabolism. Molecular cell. 2011; 44:864–77. [PubMed: 22195962]
41. Ma X, Li C, Sun L, Huang D, Li T, He X, et al. Lin28/let-7 axis regulates aerobic glycolysis and cancer progression via PDK1. Nature communications. 2014; 5:5212.
42. Sun RC, Fadia M, Dahlstrom JE, Parish CR, Board PG, Blackburn AC. Reversal of the glycolytic phenotype by dichloroacetate inhibits metastatic breast cancer cell growth in vitro and in vivo. Breast cancer research and treatment. 2010; 120:253–60. [PubMed: 19543830]
43. Sutendra G, Michelakis ED. Pyruvate dehydrogenase kinase as a novel therapeutic target in oncology. Frontiers in oncology. 2013; 3:38. [PubMed: 23471124]
44. Michelakis ED, Sutendra G, Dromparis P, Webster L, Haromy A, Niven E, et al. Metabolic modulation of glioblastoma with dichloroacetate. Science translational medicine. 2010; 2:31ra4.
45. Grassian AR, Metallo CM, Coloff JL, Stephanopoulos G, Brugge JS. Erk regulation of pyruvate dehydrogenase flux through PDK4 modulates cell proliferation. Genes & development. 2011; 25:1716–33. [PubMed: 21852536]
46. Schell JC, Olson KA, Jiang L, Hawkins AJ, Van Vranken JG, Xie J, et al. A role for the mitochondrial pyruvate carrier as a repressor of the Warburg effect and colon cancer cell growth. Molecular cell. 2014; 56:400–13. [PubMed: 25458841]
47. Marin-Valencia I, Yang C, Mashimo T, Cho S, Baek H, Yang XL, et al. Analysis of tumor metabolism reveals mitochondrial glucose oxidation in genetically diverse human glioblastomas in the mouse brain in vivo. Cell metabolism. 2012; 15:827–37. [PubMed: 22682223]
48. Sellers K, Fox MP, Bousamra M 2nd, Slone SP, Higashi RM, Miller DM, et al. Pyruvate carboxylase is critical for non-small-cell lung cancer proliferation. The Journal of clinical investigation. 2015; 125:687–98. [PubMed: 25607840]
49. Nesbit CE, Tersak JM, Prochownik EV. MYC oncogenes and human neoplastic disease. Oncogene. 1999; 18:3004–16. [PubMed: 10378696]

Author Manuscript Author Manuscript Author Manuscript Author Manuscript

50. Graves JA, Wang Y, Sims-Lucas S, Cherok E, Rothermund K, Branca MF, et al. Mitochondrial structure, function and dynamics are temporally controlled by c-Myc. PloS one. 2012; 7:e37699. [PubMed: 22629444]

51. Li F, Wang Y, Zeller KI, Potter JJ, Wonsey DR, O'Donnell KA, et al. Myc stimulates nuclearly encoded mitochondrial genes and mitochondrial biogenesis. Molecular and cellular biology. 2005; 25:6225–34. [PubMed: 15988031]

52. Morrish F, Noonan J, Perez-Olsen C, Gafken PR, Fitzgibbon M, Kelleher J, et al. Myc-dependent mitochondrial generation of acetyl-CoA contributes to fatty acid biosynthesis and histone acetylation during cell cycle entry. The Journal of biological chemistry. 2010; 285:36267–74. [PubMed: 20813845]

Author Manuscript Author Manuscript Author Manuscript Author Manuscript

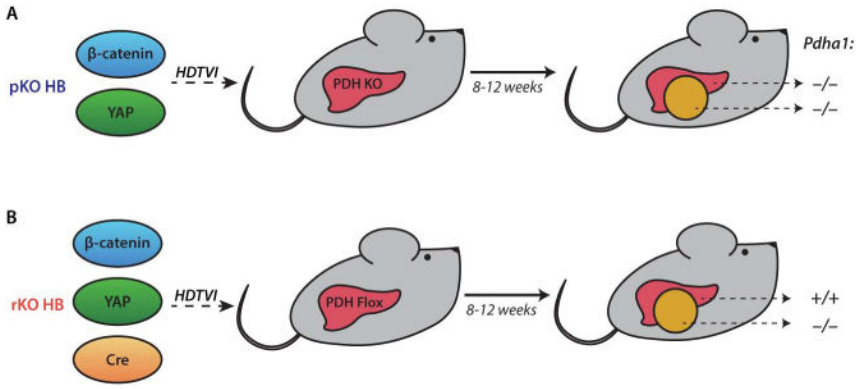

Fig 1.

Schematic for induction of hepatoblastoma in two experimental groups. (A) The first, termed “pan KO” (pKO) were progeny of matings between *Pdha1*-floxed mice and those expressing Alb-Cre, which achieved knockout of *Pdha1* in all hepatocytes. (B) The second group of mice, termed “restricted KO” (rKO) were obtained by injecting *Pdha1*-floxed mice with the β-catenin and YAP-encoding vectors in addition to a third vector encoding Cre-recombinase. In this way, the *Pdha1* gene was inactivated only in tumor cells.

Author Manuscript Author Manuscript Author Manuscript Author Manuscript

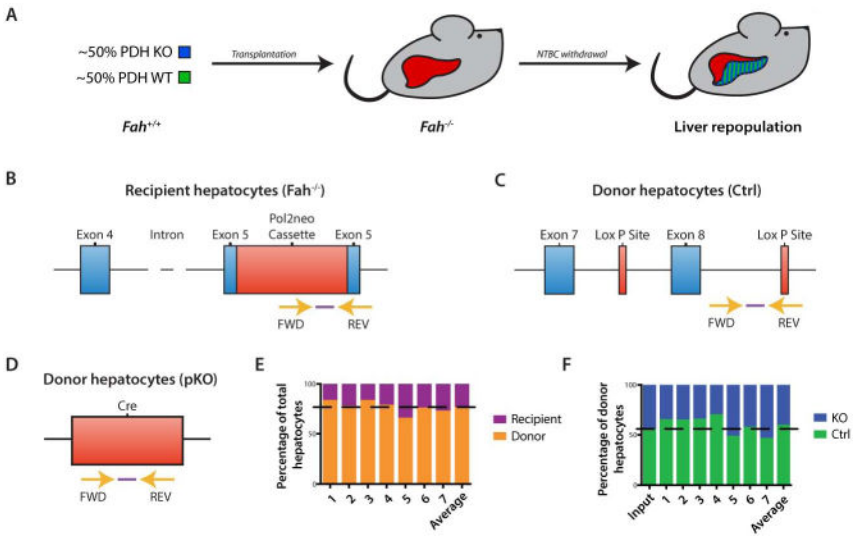

Fig. 2.

Repopulation of *fah*−/− livers by transplanted *fah+/+* control and KO hepatocytes. (A) Step-wise schematic of repopulation studies. (B) PCR scheme used to first determine the fractional contribution of *fah*−/− (recipient) and *fah+/+* (donor) hepatocytes to fully regenerated livers. Recipient donor hepatocytes were identified by real-time TaqMan-based amplification of a segment of the *neo* cassette that was embedded in the inactivated *fah* locus (see Materials and Methods). Next, the make-up of the donor hepatocyte population was determined using two TaqMan-based probes that amplified: (C) the floxed (control) donor region containing the loxP site in the intact *Pdha1* allele or (D) a segment of the Alb-Cre recombinase transgene in the *Pdha1*-KO population. Precise quantification of each population was obtained from standard curves containing varying known amounts of each of these DNAs (see Supplementary Fig. S1 A–C). (E) Results of competitive transplantation of *fah+/+* WT and KO hepatocytes into *fah*−/− FRG-NOD recipients. The fractional contribution of total donor and recipient hepatocytes of individual recipient mice is depicted after repopulation was complete between 100–130 days after transplant. (F) The contribution of control and KO populations in each of the recipient hepatocytes populations from E expressed as a fraction of the total donor population. “Input” denotes the actual makeup of the donor population.

Author Manuscript Author Manuscript Author Manuscript Author Manuscript

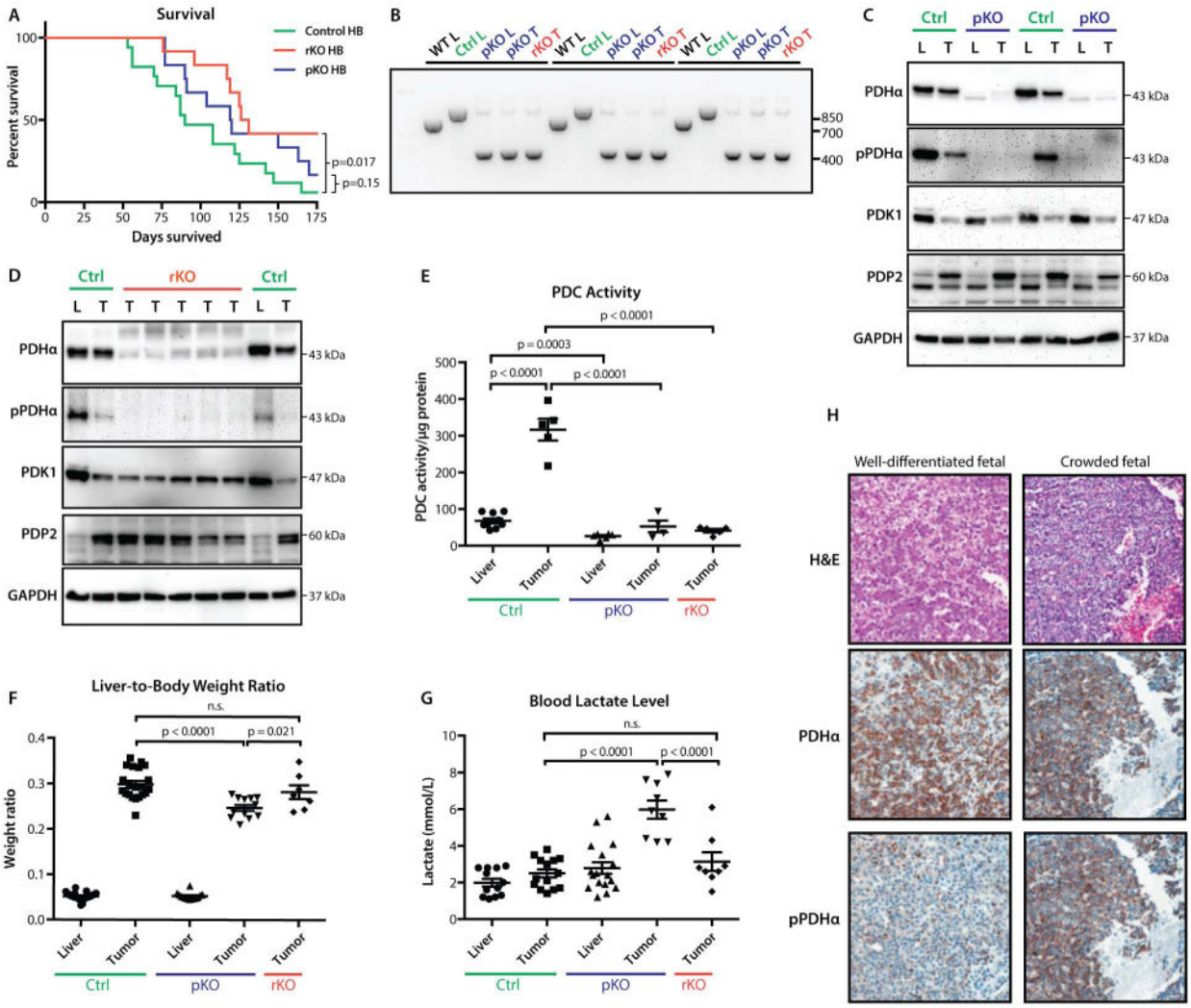

Fig. 3.

Characteristics of control and KO HBs. (A) Survival curves of control, pKO and rKO mice following HDTVI-mediated delivery of SB plasmids encoding mutant forms of β-catenin and YAP (11,12). (B) PCR results showing deletion of the *Pdha1* locus. PCR primers described in the Materials and Methods section were used to identify *Pdha1*-floxed (control/Ctrl) mice (which have two loxP sequences flanking exon 8 – lanes 2, 7, 12). The knock out was then verified in pKO livers (lanes 3, 8, 13) and tumors (lanes 4, 9, 14) and rKO tumors (lanes 4, 10, 15). Lanes 1, 6, and 11 show the results of an identical PCR performed on DNA from the livers of non-floxed mice showing amplification of a fragment lacking the loxP site. (C) Control and pKO liver and tumor lysates were assessed by immuno-blotting for total PDHα, pSer^{293}-PDH (pPDHα), PDK1, PDP2 or GAPDH, which served as a protein loading control. (D). Similar analysis as described in F performed on rKO HBs. (E) PDC enzyme activity in livers and tumors. Activities were assessed on whole tissue extracts by quantifying the release of $^{14}CO_2$ from ^{14}C-labaled pyruvate as previously described (12,14). Note that livers from rKO mice are the same as those labeled “control”. (F) Liver-to-body weight ratios of control and pKO livers, and control, rKO, and pKO HBs. Note that animals

Author Manuscript Author Manuscript Author Manuscript Author Manuscript

with pKO and rKO tumors shown here indicate a significantly larger size of tumors in the latter group. (G) Serum lactate levels in livers and tumors from the indicated groups of animals. (H). Immunohistochemical staining on typical tumor sections from human HB samples indicating much weaker overall staining of PDHα in a tumor with well-differentiated fetal morphology. Error bars denote the mean with standard error of the mean (SEM). Ctrl = control, pKO = pan-knockout, rKO = restricted KO, WT = wild type, L = liver, T = tumor.

Author Manuscript Author Manuscript Author Manuscript Author Manuscript

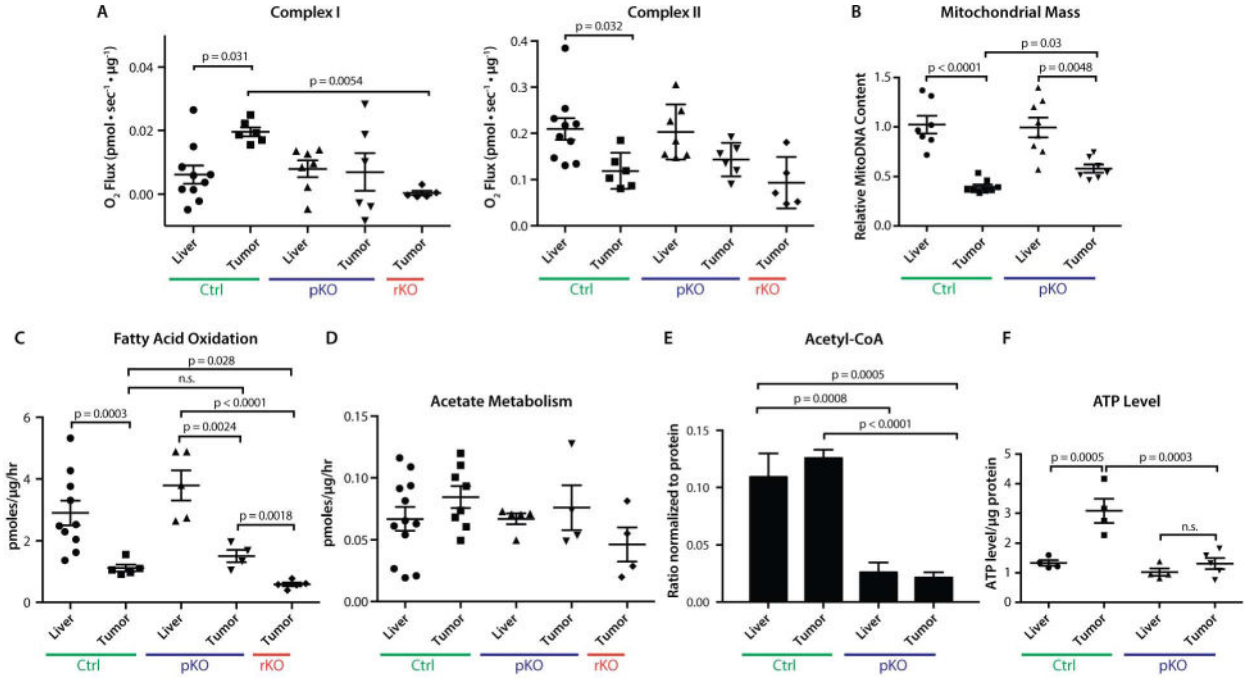

Fig. 4.

Metabolic assessment of control and KO livers and HBs. (A) Oxphos activity. Typical O_2 consumption rates (OCRs) were performed on whole liver and HB tissue lysates from the indicated groups of mice. Complex I was assessed following the sequential addition of malate, glutamine and pyruvate, and Complex II was assessed following the addition of succinate as previously described (12,14). Rotenone was then added to inhibit Complex I and to quantify its contribution to the overall OCR. Similarly, the final OCR attained after the addition of rotenone was taken as a measure of pure Complex II response. (B) Quantification of mtDNA. Total DNAs were purified from the indicated tissues and a segment of the mitochondrial genome was amplified using the TaqMan-based approach described in Supplementary Information and previously published (12). Results were normalized to those obtained from a similar TaqMan-based amplification of the nuclear-encoded apolipoprotein gene run in parallel. (C) FAO assays. Results were calculated based on the conversion of ^{3}H-labeled palmitate into $^3H_20$ (12). (D) Acetate incorporation assays. Results were calculated based in the conversion of ^{3}H-acetate in lipid-soluble products as described in Supplementary Information. (E) AcCoA levels in control and KO livers and tumors as determined by MS. n=5 independent samples/group. (F) ATP levels in livers and tumors using the ATP Lite ATP detection system. Error bars indicate the mean with SEM, except where indicated differently above. Ctrl = control, pKO = pan-knockout, rKO = restricted KO.

Author Manuscript Author Manuscript Author Manuscript Author Manuscript

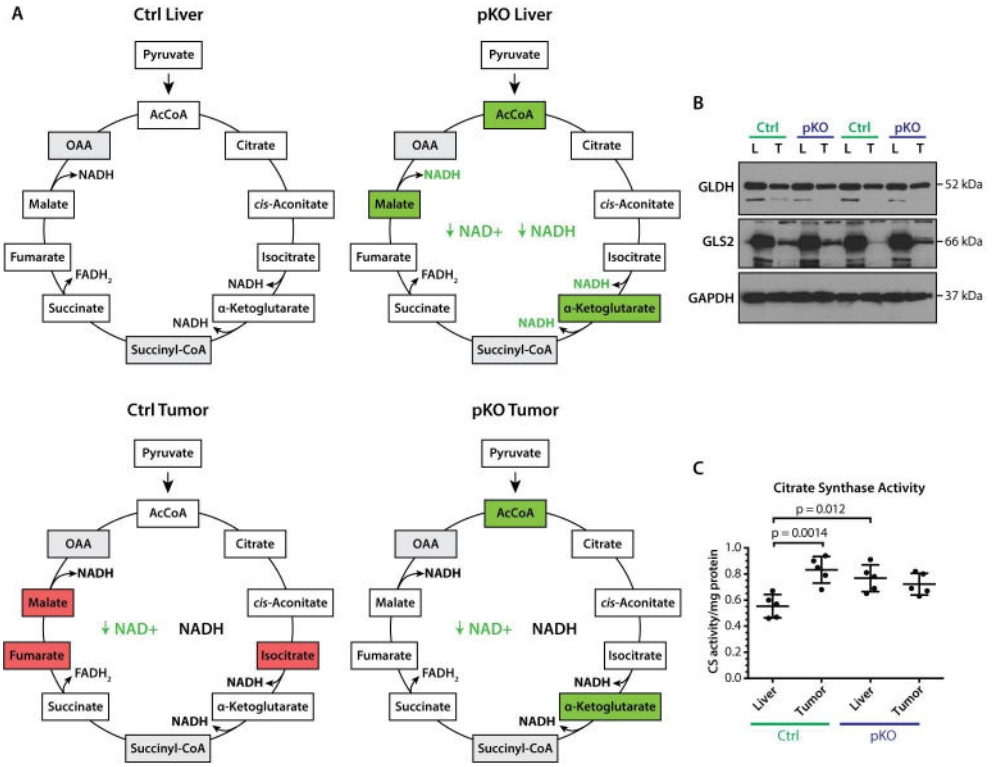

Fig. 5.

Steady-state levels of TCA intermediates in control and KO livers and tumors and the expression of key enzymes in the glutaminolysis pathway. (A) All results are from those shown in Supplementary Fig. S3 and are expressed relative to those of control liver. Red: intermediates that were present at a higher level; green: intermediates that were present at a lower level; grey: intermediates that were not measured (succinyl-CoA and oxaloacetate); black: intermediates that did not change significantly. (B) Immunoblots of representative liver and tumor samples from control and KO mice showing expression of glutamate dehydrogenase 1/2 (GLDH) and glutaminase 2 (GLS2). GAPDH served as a loading control. (C) Citrate synthase activity measured in control and pKO livers and tumors. Error bars indicate the mean +/- SEM. Ctrl = control, pKO = pan-knockout, rKO = restricted KO, L = liver, T = tumor.

Author Manuscript Author Manuscript Author Manuscript Author Manuscript

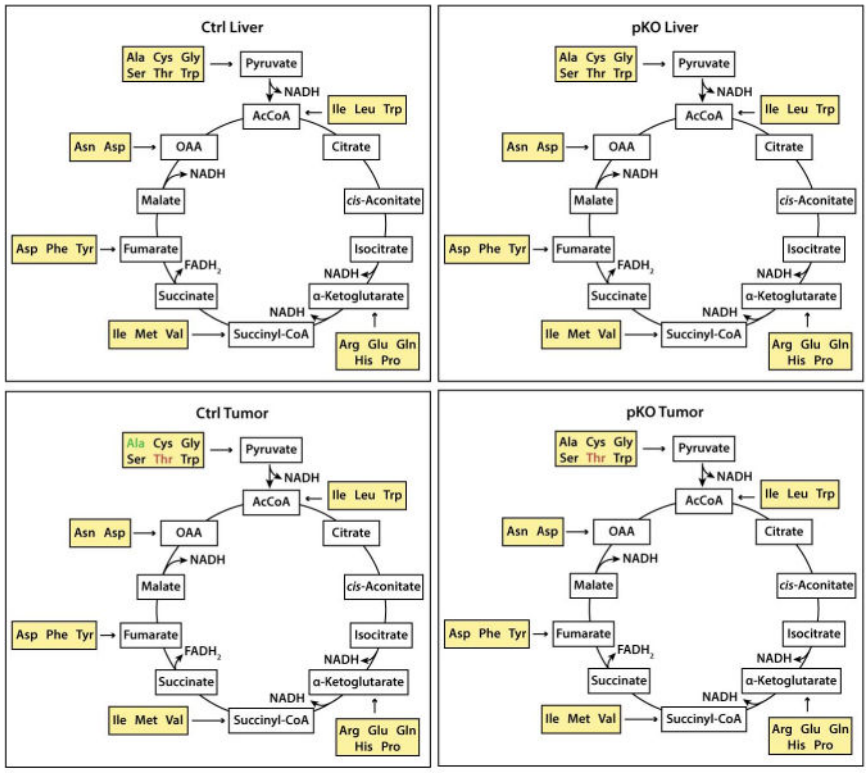

Fig. 6.

Alterations in amino acid levels in control and KO livers and tumors. Yellow boxes indicate groups of amino acids whose oxidative degradation contributes substrates directly to the TCA cycle at six different points as indicated. Lysine, which is not shown in these cartoons, can also contribute indirectly to the TCA cycle following the conversion of its end-stage product, acetoacetyl CoA, to AcCoA. Only tyrosine and asparagine were not detected in our analysis. Color-coding is the same as described for Fig. 5.